Article

Current Biology

Spatiotemporal dissociation of physical salience and stimulus evaluation in the human midbrain

Graphical abstract

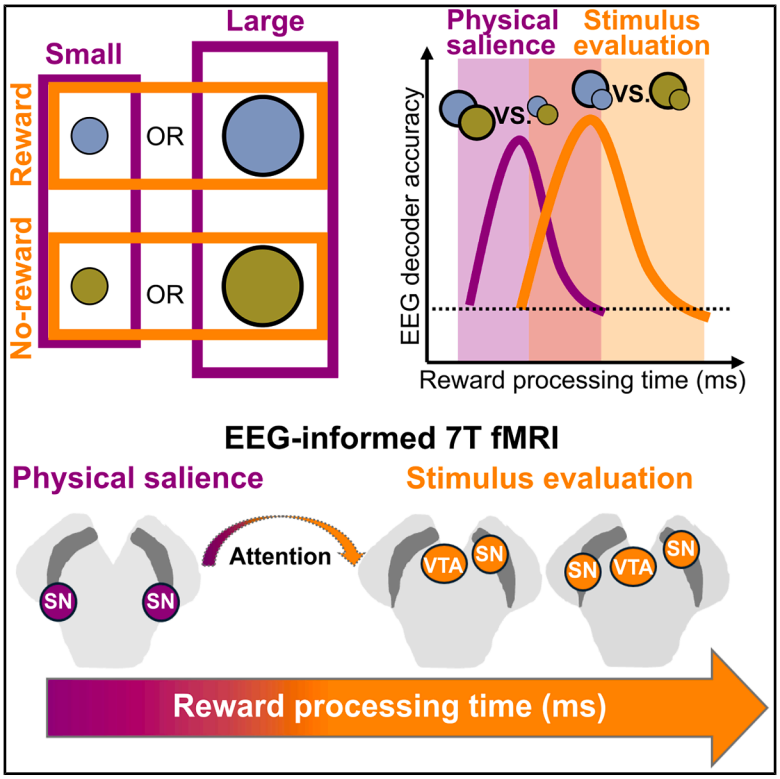

Highlights

- Spatiotemporal cascade of distinct midbrain signals during reward processing
- 7T EEG-fMRI decouples early physical salience and later evaluative midbrain signals
- Early physical salience maps to posterior SN, later evaluation to anterior SN/VTA
- Physical salience drives attention, enhancing later stimulus evaluation

Authors

Joana Carvalheiro, Paul McElhinney, Sarah Allwood-Spiers, Gavin Paterson, Shajan Gunamony, Marios G. Philiastides

Correspondence

joana.carvalheiro@glasgow.ac.uk (J.C.), marios.philiastides@glasgow.ac.uk (M.G.P.)

In brief

Carvalheiro et al. identify a spatiotemporal cascade of distinct human midbrain signals during reward processing: an early posterior substantia nigra (SN) signal reflecting physical salience, followed by an anterior SN/ventral tegmental area signal reflecting stimulus evaluation. Early salience enhances later evaluation, suggestive of an attention-guided subcortical pathway for reward processing.

Carvalheiro et al., 2025, Current Biology *35*, 5167–5178
November 3, 2025 © 2025 The Author(s). Published by Elsevier Inc.
https://doi.org/10.1016/j.cub.2025.09.013

CellPress

Current Biology

CellPress
OPEN ACCESS

Article

Spatiotemporal dissociation of physical salience and stimulus evaluation in the human midbrain

Joana Carvalheiro,[1,4,*] Paul McElhinney,[2] Sarah Allwood-Spiers,[2,3] Gavin Paterson,[1] Shajan Gunamony,[2] and Marios G. Philiastides[1,*]

[1]School of Psychology and Neuroscience, University of Glasgow, Glasgow G12 8QB, UK
[2]Imaging Centre of Excellence, University of Glasgow, Glasgow G51 4LB, UK
[3]Department of Clinical Physics and Bioengineering, NHS Greater Glasgow and Clyde, Glasgow G51 4LB, UK
[4]Lead contact
*Correspondence: joana.carvalheiro@glasgow.ac.uk (J.C.), marios.philiastides@glasgow.ac.uk (M.G.P.)
https://doi.org/10.1016/j.cub.2025.09.013

SUMMARY

The brain must detect and evaluate rewards amidst multiple stimuli to generate adaptive behavior. Physically salient stimuli draw greater attention, potentially influencing their subsequent evaluation. An influential framework proposes that rewards are processed through a two-component dopaminergic response: an early, value-agnostic salience signal, followed by a partially overlapping but temporally lagged signal reflecting stimulus evaluation. Yet, evidence for this framework in humans is lacking due to spatiotemporal limitations of neuroimaging methods. Using bespoke simultaneous 7T functional magnetic resonance imaging (fMRI)-electroencephalogram (EEG) developments, we decoupled reward-anticipatory midbrain signals with distinct spatiotemporal profiles: an early signal in posterior substantia nigra (SN) consistent with physical salience, followed by a lagged signal in anterior SN and ventral tegmental area, likely reflecting evaluative processes such as value and/or motivational salience. We also demonstrate that the early physical salience signal enhances this later evaluative response, offering the first evidence of attention-guided reward processing in the human midbrain.

INTRODUCTION

Learning the relationships between stimuli and the rewards they predict is critical for adaptive behavior. However, animals often encounter a multitude of reward-predicting stimuli, requiring detection and subsequent prioritization of those that maximize reward to ensure survival. Reward-predictive stimuli often differ in their physical salience (e.g., size and contrast), with more salient stimuli attracting greater attention and leading to better detectability. In turn, reorienting of attention presents itself as a potentially meaningful mechanism through which stimuli are prioritized for processing to avoid missing potential rewards.

In line with this, a prominent theoretical framework proposes that reward processing is driven by dopaminergic midbrain responses that evolve over time from an early salience signal to a later evaluative signal.[1] In this two-component dopaminergic reward response, the first component is thought to reflect an initial, brief, unselective sensory detection, which then transitions into a second component representing reward evaluation. Temporally, these two components—physical salience and stimulus evaluation—are proposed to occur rapidly and may partially overlap in time.[1,2] While this framework makes explicit predictions about the temporal evolution of these two components, it does not offer specific predictions about their spatial organization in the midbrain.

Previous non-human animal studies suggest that different populations of dopamine neurons in the midbrain may preferentially encode different aspects of stimulus evaluation. For example, value signals—reflecting how good or bad a stimulus is—are typically found in the ventromedial substantia nigra (SN) and ventral tegmental area (VTA), while motivational salience—responses to stimuli predicting either good or bad outcomes—has been primarily localized in the dorsolateral SN.[3–6] However, it remains unknown whether early, value-agnostic responses to physically salient stimuli are not only temporally but also spatially segregated from these later evaluative responses in the midbrain. Demonstrating a temporal and spatial dissociation between physical salience and evaluation-related signals would not only provide critical insight into the functional architecture of the human midbrain but also offer an important extension of the two-component framework, which currently focuses on temporal predictions alone.

Despite the theoretical implications of such spatiotemporal dissociations in reward processing, empirical evidence remains scarce, even in non-human studies. Firstly, decoupling these signals in time—given their partially overlapping nature—requires millisecond temporal precision, which some cellular imaging techniques cannot provide. By contrast, high-temporal resolution electrophysiological studies focusing on single-unit recordings may not accurately capture the full extent and spatial segregation of these signals. Finally, only a few studies[2] have explicitly manipulated physical salience and stimulus evaluation orthogonally, a critical requirement to avoid conflating these signals into a mixed aggregate representation due to their temporal overlap.

This is an open access article under the CC BY license (http://creativecommons.org/licenses/by/4.0/).

Physical salience offers a tractable and well-controlled way to elicit the first component of the two-component dopaminergic response. As a sensorial feature that captures attention, it provides a means to isolate early dopaminergic activity that is independent of stimulus evaluation.[1] For example, variations in cue size not only drive stronger early visual cortical responses[7,8] but also produce temporally precise electroencephalogram (EEG) signals, which can be leveraged to test the time course of physical salience and subsequent stimulus evaluation. When combined with high-spatial resolution functional magnetic resonance imaging (fMRI), these temporal signals can also be mapped onto their corresponding spatial locations within the midbrain.[9]

While human studies have provided some insight into midbrain reward-processing components, evidence for their temporal and spatial dissociations remains limited. Most have examined either the timing[10–13] or the spatial localization[14–20] of reward-related signals, but not both. As such, the literature is currently lacking a comprehensive view of how early physical salience and later evaluative signals emerge—and possibly interact—in dopaminergic pathways. A key challenge in testing this framework in humans lies in the limitations of current neuroimaging techniques, which often lack the necessary temporal and spatial resolution needed to decouple these midbrain signals.

To overcome these challenges, we combine EEG with ultra-high-field 7T fMRI using an in-house bespoke EEG-fMRI head coil[21] and custom-made MR-compatible EEG caps. We first leverage the high-temporal precision of the EEG to understand how physical salience and stimulus evaluation unfold in time via a machine-learning multivariate decoding approach,[22,23] which produces endogenous trial-by-trial response variability associated with the two signals. We then use these single-trial EEG responses to build EEG-informed fMRI predictors to decouple the relevant midbrain correlates for each of the early physical salience and later evaluative signals.

The core of our approach rests on the idea that while EEG is driven primarily by cortical regions found near the recording sensors, distant subcortical structures can still be revealed, provided their blood-oxygen-level-dependent (BOLD) activity covaries systematically with that of the cortical sources of our EEG signals.[9,24–27] This is achieved through high-resolution 7T fMRI, with a sequence tailored for enhanced sensitivity in imaging the SN/VTA[28] compared with 3T fMRI. Notably, such spatiotemporal decoupling is not possible with conventional fMRI analysis, as the slow BOLD signal cannot dissociate signals emerging temporally in rapid succession.

In short, by fusing EEG with 7T fMRI, we succeeded in decoupling the temporal cascade of early physical salience and later evaluative responses in the human midbrain during reward processing. Importantly, these temporally distinct signals were also spatially segregated within the SN/VTA. Moreover, we show that early and late signals interact, with physical salience enhancing subsequent stimulus evaluation—likely through increased attentional allocation.

RESULTS

Reward-anticipation task performance

To dissociate physical salience from stimulus evaluation, we used a modified version of the monetary incentive delay task[29] (Figures 1A and 1B) in which we orthogonally manipulated two features of the cue: size and reward contingency. Physical salience was manipulated by varying cue size (large versus small circles)—a basic, value-agnostic, attention-capturing feature—intended to elicit early responses. Stimulus evaluation was manipulated by varying reward expectation, using colored cues (blue or yellow circles) that predicted either a reward or no reward. In this task, stimulus evaluation was therefore operationalized as increased neural activation for reward- versus no-reward-predictive cues,[30] which may include both stimulus value and motivational salience components.

Specifically, on each trial, participants viewed a single-colored cue (blue circle or yellow circle) that predicted either a reward (£10) or no reward (£0). Half of the cues were large, and half were small, with cue size and reward contingency varying independently across trials. After a variable delay, a target briefly appeared, and participants were instructed to press a key as quickly as possible. For reward-predictive cues, hitting the target in time led to a £10 reward, and for no-reward cues, the outcome was always £0, regardless of response speed.

Participants tracked the reward-predictive value of each symbol by responding faster to targets following reward-predictive symbols ($p < 0.0001$, $d = -1.59$, paired t test; Figure 1C), regardless of their physical salience ($p = 0.25$, $d = 0.24$, paired t test; Figure 1C). This pattern of behavior aligns with previous findings showing that reward anticipation engages sustained motor-preparation and cognitive-control processes, biasing actions toward reward-predictive cues, even after the cue has disappeared.[31–33] By contrast, visual salience is thought to operate via rapid, stimulus-driven orienting mechanisms that decay quickly after cue offset[34] and may not influence responses at the time of a delayed target.

Given that the response target was temporally delayed from cue presentation (to avoid motor confounds in the analysis of the neuroimaging data) and was designed to primarily track responses to reward anticipation, we wanted to confirm that larger stimuli indeed captured greater attention than smaller stimuli at the time of the cue presentation. To this end, we performed an independent experiment in which each participant ($n = 24$) completed two tasks: one requiring an immediate response to large and small cues, and another replicating the main task's delayed-response structure, in which responses were made to a delayed target after the large and small cues.

Participants responded significantly faster to large cues than to small cues in the immediate-response task ($p = 0.003$, $d = 0.66$, paired t test; Figure 1D). This effect was absent in the delayed-target task ($p = 0.66$, $d = 0.091$, paired t test; Figure 1D). A repeated-measures ANOVA confirmed a significant interaction between cue size and task ($p = 0.013$, partial $\eta^2 = 0.24$; Figure 1D). These findings validate our physical salience manipulation: larger cues facilitate immediate behavioral responses but exert limited behavioral influence when the response is temporally separated from cue presentation, as in our main neuroimaging task.

Temporal dissociation of physical salience and stimulus evaluation

To identify the relative timings of physical salience and evaluative signals, we used single-trial multivariate decoding analysis of the

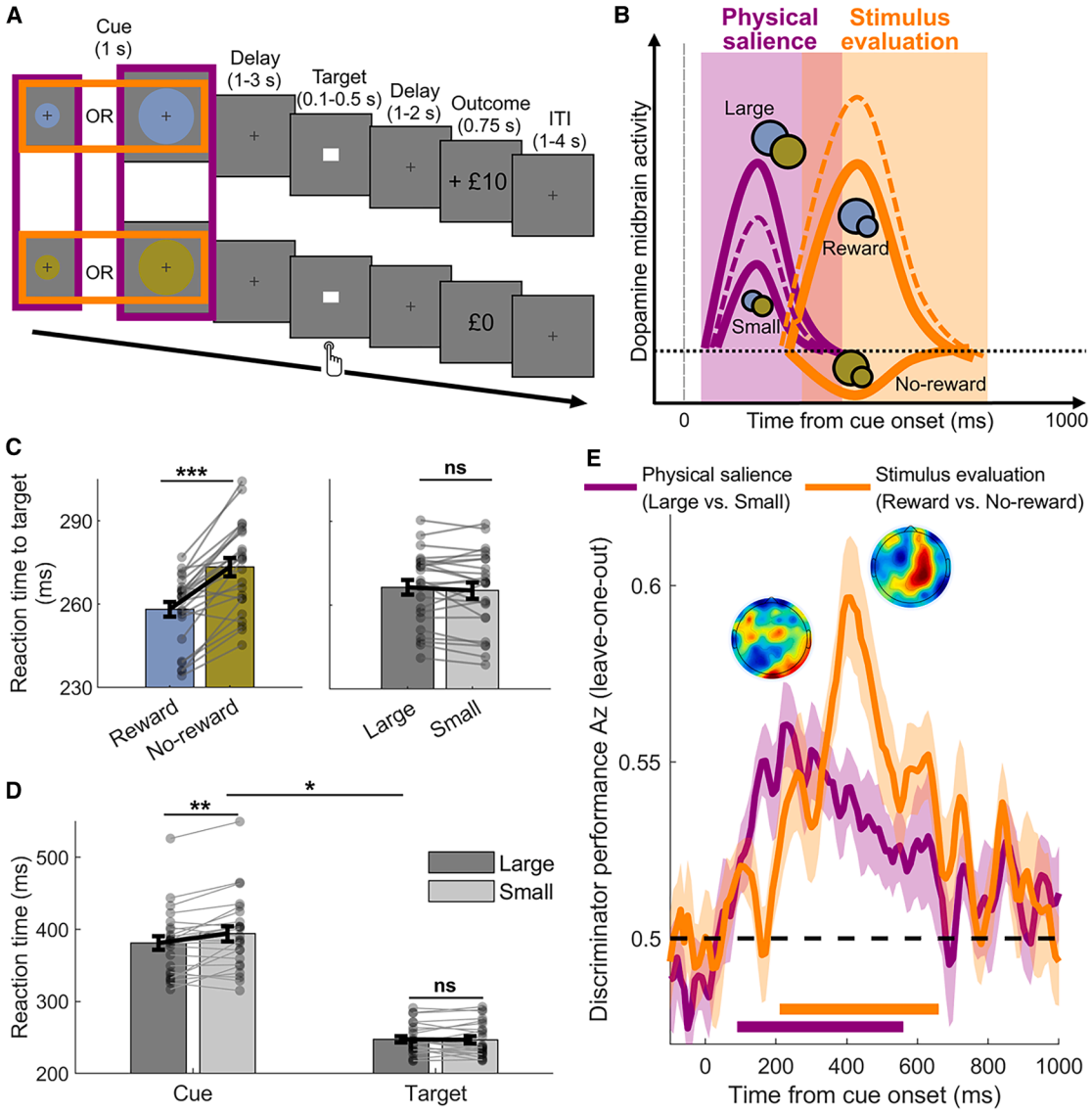

Figure 1. Experimental task, predictions, and behavioral and EEG measures

(A) In each trial, participants observed a colored cue (large or small) predicting either a reward (win) or no reward (nothing), contingent on their speeded response to a variable-duration target (white square).

(B) In line with the two-component framework, we predicted that dopamine midbrain neurons would initially respond more strongly to larger cues than smaller ones (early physical salience signal, purple) and subsequently increase firing for reward cues while decreasing for no-reward cues (later stimulus evaluation signal, orange). Dashed lines show predicted differences between the two conditions.

(C) Reaction times to the target after reward versus no-reward cues (left) and large versus small cues (right). Dots represent individual data ($n = 24$), and error bars are mean ± SEM (***$p < 0.001$, ns $p > 0.05$, paired t tests).

(D) In an independent sample ($n = 24$), we assessed reaction times to large and small cues, as well as to targets that followed large and small cues after a variable delay (1–3 s), the latter using the same structure as in the EEG-fMRI task. Dots represent individual data, and error bars are mean ± SEM (**$p < 0.01$, *$p < 0.05$, ns $p > 0.05$, paired t tests, and on top the interaction task × size from ANOVA repeated-measures).

(E) Multivariate decoding accuracy (A_z) for physical salience (large versus small cues) and stimulus evaluation (reward versus no-reward cues), with a temporal profile consistent with the predicted differences in (B) (dashed lines) and scalp topographies showing largely distinct spatial patterns for physical salience (160–220 ms) and stimulus evaluation (400–460 ms). Colored bars beneath the plot indicate time windows where decoding accuracy is significantly above chance (one-tailed test against 0.5, with a cluster-based permutation test, 1,000 permutations; cluster-forming threshold $\alpha = 0.05$; cluster-level $\alpha = 0.01$, corrected for multiple comparisons). Central lines show the mean across participants, with shaded areas indicating ± SEM. The dotted line represents chance-level decoding accuracy.

Also see Figure S1 for time courses of EEG component amplitudes in each individual condition, providing a comparison with the model predictions in Figure 1B. Also see Figure S2 for results from an EEG-only control experiment that temporally decoupled stimulus evaluation signals (value and motivational salience).

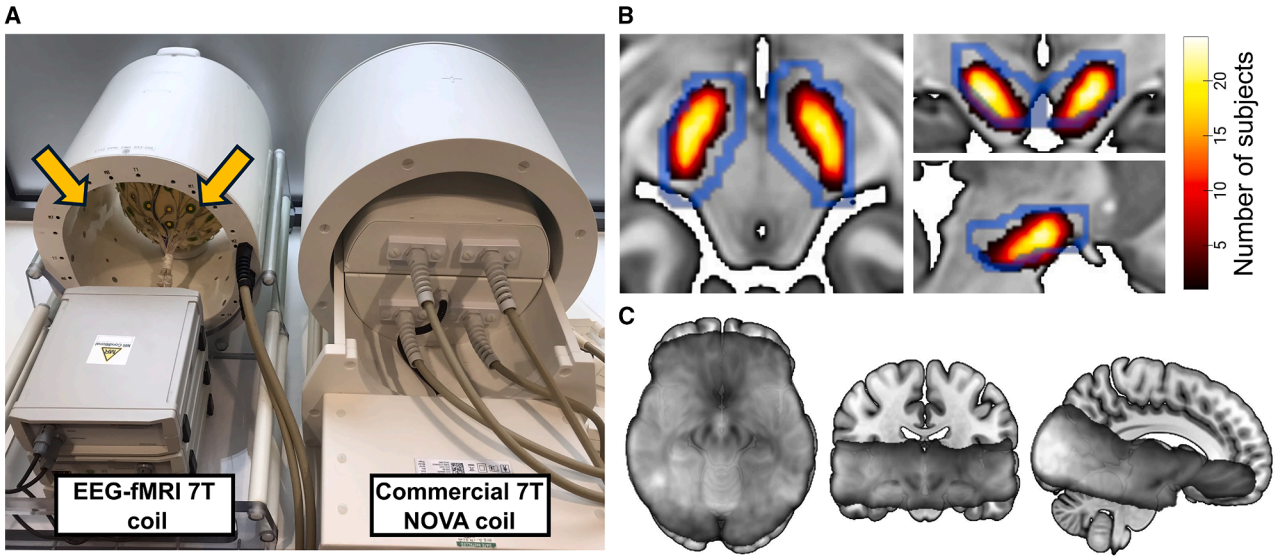

Figure 2. EEG-fMRI equipment and image registration quality

(A) The in-house coil we built for simultaneous EEG-fMRI at 7T (left). Unlike the commercial 7T coil (right), which features an electronics bay at the back, our coil features an open design (electronics fully integrated into the coil), allowing direct connection of the EEG cap cables to the EEG amplifiers through the back opening (indicated by the yellow arrows).

(B) Overlap of manually delineated substantia nigra (SN) masks on the transforms from EPI to MNI space across participants ($n = 24$). Lighter colors indicate regions of greater overlap among participants. The blue outline represents the boundaries of the atlas-generated SN mask, which is later used for cluster correction analysis at the group level.

(C) Sum of individual transforms from the EPI space to MNI space across all participants, overlaid on an MNI template. More defined (blurred/lighter) structures indicate a higher (lower) degree of overlap across individuals. Note, the midbrain structures of interest (SN/VTA) are very well delineated. EPI, echo planar imaging; MNI, Montreal Neurological Institute.

Also see Figure S3 for details of the midbrain field of view, registration, and comparisons between 3T and 7T measurements.

EEG signals time-locked to cue (stimulus) onset, separately for each participant. Each analysis estimates sensor weights separately for physical salience and stimulus evaluation, which maximally discriminate between large and small cues (physical salience) and between reward and no-reward cues (stimulus evaluation) (see STAR Methods; Equation 1). By applying these spatial weights to single-trial EEG data, we produced a measurement of the trial-wise amplitudes for each signal, which we subsequently used to build parametric EEG-informed fMRI regressors to tease apart the cascade of physical salience and stimulus evaluation in the midbrain.

As predicted, EEG analyses revealed an early physical salience component that peaked at 230 ms, with decoding accuracy remaining significantly above chance from 90 to 560 ms ($p < 0.01$, cluster-based permutation test corrected; Figure 1E). A later, partially overlapping component associated with stimulus evaluation peaked at 410 ms, with decoding accuracy remaining above chance from 210 to 660 ms ($p < 0.01$, cluster-based permutation test corrected; Figure 1E, also see Figure S1). The two components also showed distinct scalp topographies (Figure 1E), reaffirming they reflect separate neural signals.

Since our late component was produced by discriminating between reward versus no-reward (neutral) cues, we wanted to confirm that this component captures value even when motivational salience is held constant (as rewarding cues might be perceived as more motivationally salient than neutral ones). To this end, we conducted a control analysis using an independent stand-alone EEG dataset ($n = 24$) collected with the same task but with additional punishment-predictive cues and constant physical salience (see STAR Methods for further details on the task). First, we decoded responses to reward versus punishment cues, which are matched for motivational salience but differ in value. In the same 210–660 ms time window identified above, decoding accuracy remained robustly above chance ($t(23) = 4.31$, $p < 0.001$, d = 0.88, one-sample t test against 0.5; see Figure S2A). This indicates that the late evaluative response includes a value component, even when motivational salience is held constant. Additionally, decoding between motivationally salient cues (reward and punishment) versus neutral cues revealed an overlapping signal ($t(23) = 6.43$, $p < 0.001$, d = 1.31, one-sample t test against 0.5; see Figure S2B). This analysis supports the interpretation that the late evaluative signal may include contributions from both value and motivational salience.

Together, these findings establish a clear temporal separation in human EEG between an early physical salience signal and a later evaluative signal—precisely as predicted by the two-component dopaminergic reward response.[1] We next asked whether these components are not only temporally distinct but also spatially segregated within the human midbrain, specifically in the SN/VTA. To address this, we used a simultaneous 7T EEG-fMRI fusion approach.

Distinct spatiotemporal dynamics of physical salience and stimulus evaluation in the midbrain

After validating the data quality in SN/VTA using our custom-built 7T EEG-fMRI coil (Figure 2, also see Figure S3), we first

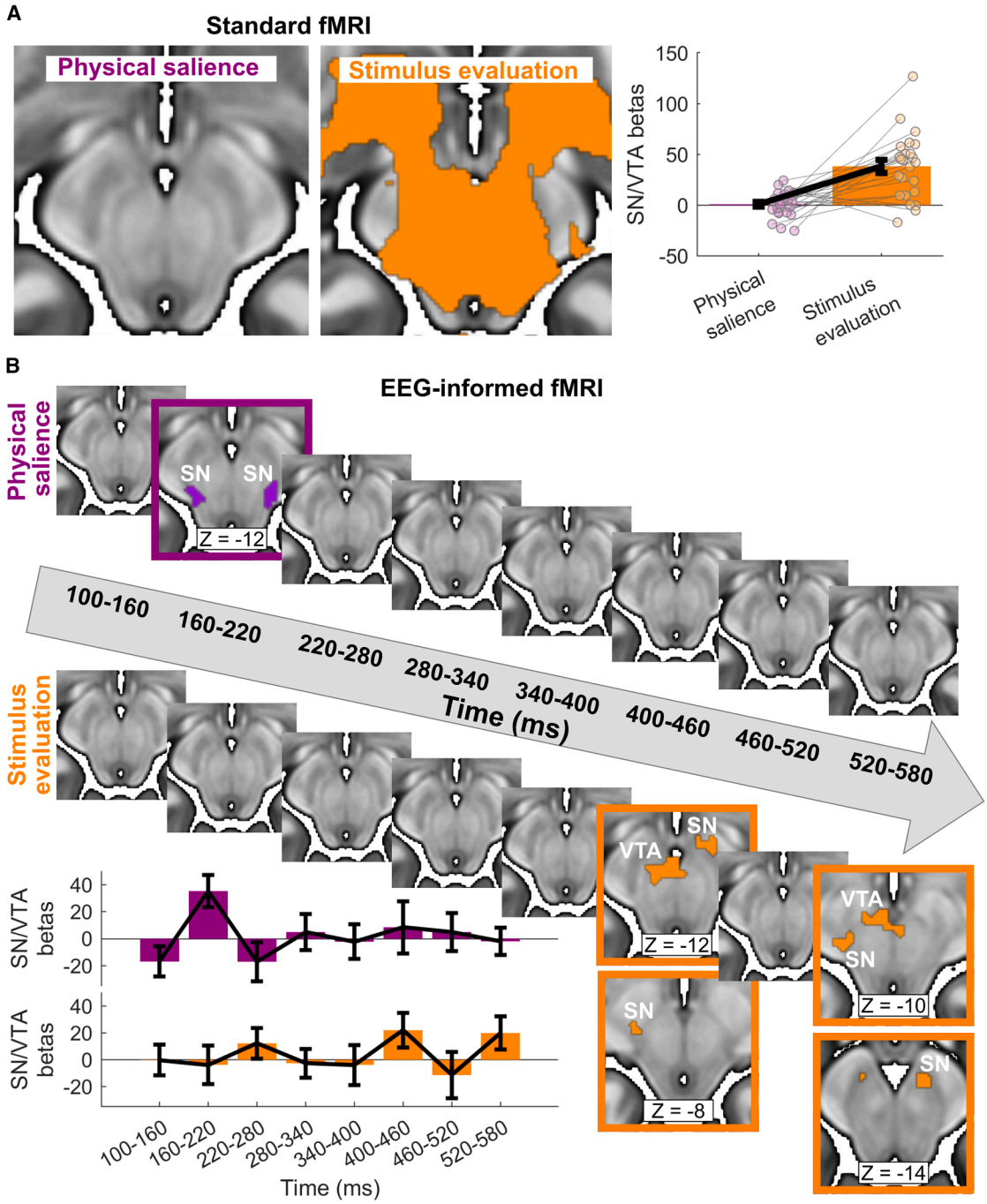

Figure 3. Spatiotemporal dissociation of physical salience and stimulus evaluation in the midbrain

(A) Standard fMRI activations. Activations for physical salience (large > small cues) and stimulus evaluation (reward > no-reward cues) using standard categorical regressors (*Z* scores > 2.3, cluster corrected). Bar plots depict individual BOLD estimates (i.e., betas) for the two contrasts within the SN/VTA mask ($n = 24$), with error bars representing the mean ± SEM.

(B) EEG-informed fMRI activations within SN/VTA. Activations for physical salience and stimulus evaluation are analyzed using parametric regressors based on single-trial EEG amplitude variability over 60 ms time windows (all *Z* scores > 2.3, cluster corrected). Bar plots show BOLD estimates for each window within the SN/VTA mask, with error bars representing the mean ± SEM. *Z* coordinates refer to standard MNI brain space.

Also see Figures S4 and S5 for complementary analyses, including lower-threshold EEG-fMRI maps, time-window-specific effects, overlap of late evaluation clusters, motor-control EEG/EEG-fMRI analyses, and superior colliculus responses to physical salience. Also see Table S1 for activation coordinates.

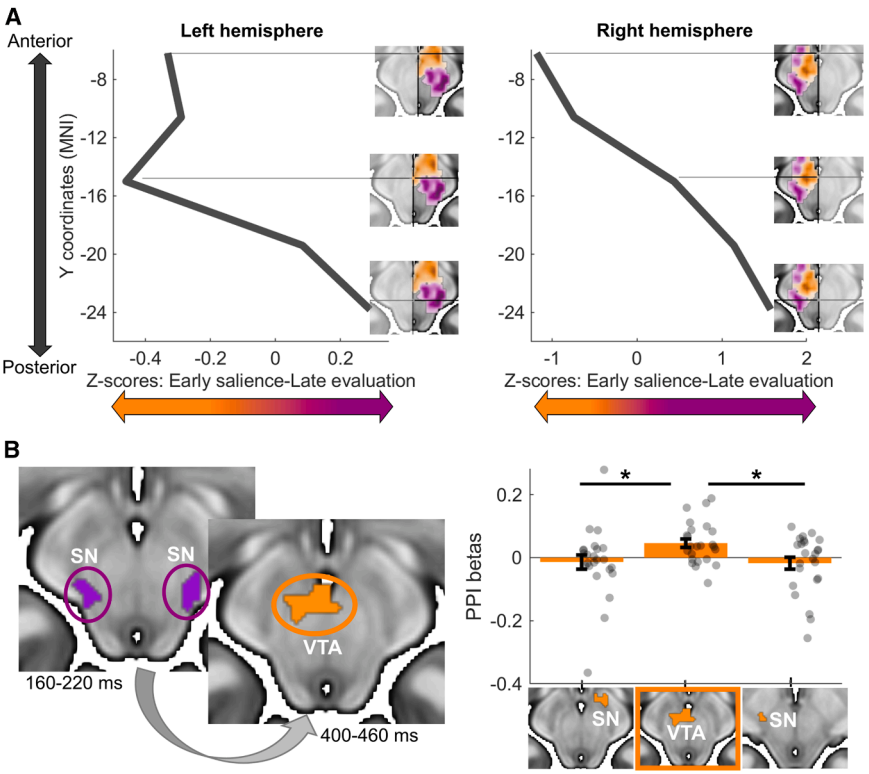

Figure 4. Spatial gradients and functional coupling between physical salience and stimulus evaluation signals in the SN/VTA

(A) Group-level differences in *Z* scores between physical salience (160–220 ms) and stimulus evaluation (400–460 ms) along the posterior-anterior (*y*) axis in MNI space, within the SN/VTA anatomical mask ($n = 24$). Voxelwise *Z* scores were averaged across six *y*-coordinate bins and displayed separately for the left (left) and right (right) SN/VTA. Insets show unthresholded *Z* score differences across three exemplary axial slices. Dark purple indicates stronger responses to physical salience compared with stimulus evaluation (lighter purple indicates smaller differences), while dark orange indicates stronger responses to stimulus evaluation compared with physical salience (lighter orange indicates smaller differences).

(B) Psychophysiological interaction (PPI) analysis showing functional connectivity between early physical salience clusters (seed) and an evaluation-related cluster in the VTA. Coupling strength increased with EEG amplitudes of evaluation signals at 400–460 ms. Bar plots (right) show individual BOLD estimates from PPI analysis in three evaluation-related subclusters identified via EEG-informed fMRI during the 400–460 ms window. Dots represent individual data ($n = 24$), and error bars are mean ± SEM (*$p < 0.05$, paired *t* tests).

performed a standard (stand-alone) fMRI analysis to confirm that the reward-anticipation task elicited SN/VTA activations.[29,35] This analysis included categorical regressors for physical salience (large > small) and stimulus evaluation (reward > no reward). We found extensive midbrain activations for the stimulus evaluation contrast, but no activations for physical salience (Figure 3A). Critically, however, these conventional fMRI contrasts reveal only categorical differences and do not capture endogenous neural fluctuations, which may offer additional explanatory power. Similarly, this conventional fMRI approach does not account for the relative timings of the early physical salience and late evaluative signals, which evolve in rapid succession, as predicted by the two-component framework (Figure 1B) and empirically demonstrated in our EEG analysis (Figure 1E).

To address these shortcomings, we exploited the endogenous single-trial variability in the EEG amplitudes of the early (physical salience) and late (stimulus evaluation) signals, using short 60 ms window increments. These trial-wise amplitudes were used to build separate parametric EEG-informed fMRI regressors at different time points relative to the cue, allowing us to examine how they might explain dynamic changes in the SN/VTA BOLD signal, over and above what could be conferred by stand-alone fMRI. Note that it is ultimately the trial-by-trial amplitude modulation of the different EEG-informed fMRI regressors, not the timing of the EEG signals themselves, that enables the temporal decoupling of the BOLD signal.

Crucially, the EEG-informed fMRI analysis revealed a clear temporal and spatial dissociation between the two signals. Unlike the standard fMRI analysis, we detected physical salience clusters in the SN driven by EEG signal amplitudes obtained from an early time window (160–220 ms), while evaluation-related signals emerged in the SN/VTA driven by EEG signal amplitudes at later time points (400–460 and 520–580 ms) (Figure 3B). In addition to these distinct temporal patterns, we observed a spatial dissociation across the two signals. Physical salience clusters were localized posteriorly within the SN, whereas stimulus evaluation clusters were predominantly located in the anterior SN and VTA, with no spatial overlap between the two signals (Figure 3B; also see Figure S4A and Table S1).

Furthermore, we found that the later evaluative response (400–460 ms) captured the activation of unique voxels in the anterior SN and VTA, rather than an overall increase in SN/VTA activation strength (Figures S4B–S4D). We further verified that clusters associated with the later time windows (400–460 and 520–580 ms) showed partial spatial overlap and correlated activity (Figures S4E–S4G), indicating that the evaluative process was more sustained over time. Since participants responded faster to reward-predictive cues, we performed additional analyses to rule out that the observed activations were driven by (pre)motor activity (Figures S5A and S5B). Additionally, we demonstrated that fusing EEG with fMRI at 7T enhanced statistical power, relative to standard fMRI analysis, and enabled the detection of deeper structures by detecting physical salience (but not stimulus evaluation) signals in a "control" region, namely the superior colliculus (Figures S5C–S5F), which is a midbrain structure well-known for responding to the physical salience of visual input, with projections to the SN.[36,37]

Finally, motivated by non-human work showing that dopamine neurons with distinct stimulus-evaluation tuning profiles—ranging from motivational salience to value—are spatially

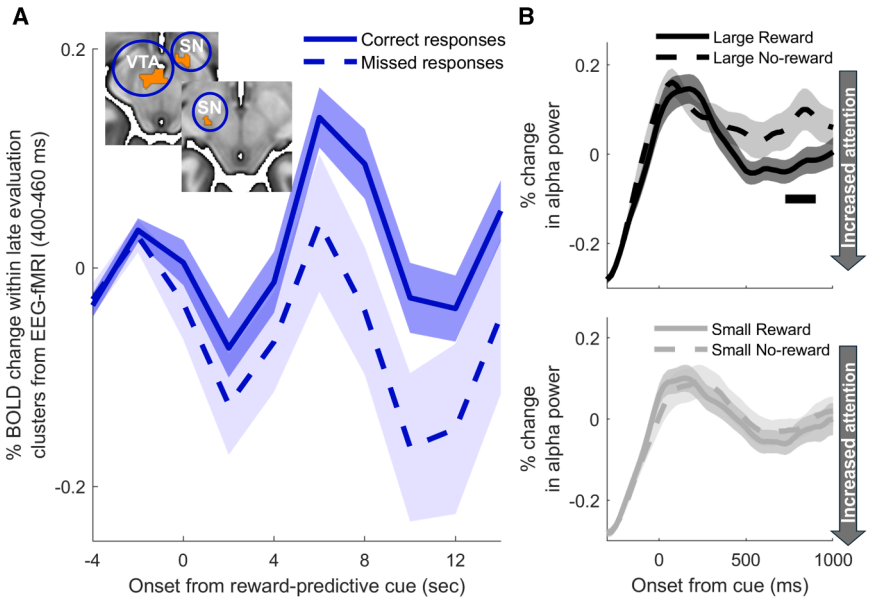

Figure 5. BOLD SN/VTA responses as predictors of accuracy, and alpha-band power as an EEG marker of attention

(A) Time course of BOLD signal % change within late evaluation-related clusters in the SN/VTA, identified via EEG-informed fMRI during the 400–460 ms post-cue window. BOLD responses locked at reward-predictive cues onset are shown separately for correct (solid line) and missed (dashed line) trials. The inset shows anatomical locations of the stimulus-evaluation clusters within the SN/VTA.

(B) Time course of alpha-band (8–12 Hz) power changes over evaluation-related EEG channels, shown as a function of cue size and reward magnitude. The top panel displays trials with large cues that anticipated either reward (solid line) or no reward (dashed line), and the bottom panel displays trials with small cues that also anticipated either reward (solid line) or no reward (dashed line). Reductions in alpha power, likely reflecting increased attentional engagement, are indicated by vertical arrows. Black bars beneath the top panel indicate time windows where reward and no-reward conditions differed significantly for large cues (two-tailed test, cluster-based permutation test, 1,000 permutations; cluster-forming threshold $\alpha = 0.05$; cluster-level $\alpha = 0.05$, corrected for multiple comparisons). In (A) and (B), central lines show the mean across participants ($n = 24$), with shaded areas indicating ± SEM.

organized along a dorsolateral-to-anteromedial gradient in the SN/VTA,[5,6,38] we asked whether a spatial gradient might also apply to our physical salience and stimulus evaluation signals in the human SN/VTA. To do so, we regressed voxel-wise group activation differences (physical salience minus stimulus evaluation) against the posterior-anterior (y axis) coordinate. In the right SN/VTA, this posterior-to-anterior gradient was significant (regression slope, $\beta = -0.17$, $p = 0.0018$; Figure 4A), whereas no reliable gradient was observed in the left hemisphere (regression slope, $\beta = -0.037$, $p = 0.095$; Figure 4A). Moreover, the gradient in the right SN/VTA was significantly steeper than in the left (regression slope β difference $= -0.13$, $p < 0.001$). These effects were confirmed at the single-subject level, where a consistent gradient was evident in the right SN/VTA (regression slope mean, $\beta = -0.038$, $p = 0.0051$), but not in the left (regression slope mean, $\beta = -0.0066$, $p = 0.61$).

Additionally, we examined a lateral-to-medial gradient by regressing salience-evaluation activation differences onto lateral-medial (x axis) coordinates. A significant positive gradient emerged in the right SN/VTA (regression slope $\beta = 5.2$, $p = 0.020$), but not in the left (regression slope $\beta = -1.21$, $p = 0.85$). However, the difference in slopes between hemispheres did not reach significance (regression slope β difference $= 0.18$, $p = 0.070$). These findings suggest a posterior-lateral to anterior-medial transition from physical salience to stimulus evaluation signals in the right SN/VTA. Thus, our data reveal a novel midbrain pathway in which early physical salience signals in dorsal SN may influence subsequent evaluative processes in anterior-medial SN/VTA regions.

In sum, these results reveal a spatiotemporal organization of reward-anticipation signals in the human midbrain. Uniquely enabled by the combination of EEG and 7T fMRI, our findings provide empirical support for the temporal predictions of the two-component framework while also extending it by showing a spatial segregation between early physical salience and later evaluation-related signals in the human SN/VTA.

Interaction between early physical salience and later stimulus evaluation

Finally, the two-component framework proposes that early physical salience can facilitate the later evaluation of reward-predictive stimuli.[1] To test this idea, we examined whether trial-by-trial fluctuations in early physical salience-related midbrain activity were positively coupled with subsequent evaluation-related responses. Specifically, we performed psychophysiological interaction analysis, using the early salience cluster as the seed region and the single-trial EEG amplitudes of the later evaluative component (within the 400–460 ms time window) as the psychological regressor. We found a positive association between the early physical salience signal and the strength of the later evaluation-related activation, particularly within a VTA subcluster ($p = 0.0025$, $d = 0.69$; one-sample t test against zero). This interaction effect in the VTA was significantly stronger than in the other two clusters (both $p < 0.03$; paired t tests; Figure 4B).

Moreover, to assess the behavioral relevance of the late evaluation-related activity, we tested whether BOLD activation in the SN/VTA clusters covarying with the late EEG component (400–460 ms) predicted task performance. Activation during reward-predictive cue presentation was significantly greater on trials in which participants subsequently responded to the target on time compared with trials with missed responses ($Z = 2.03$, $p = 0.042$; Wilcoxon signed-rank test, Figure 5A). Additionally, trial-wise modeling revealed a trend-level association between SN/VTA activation and response accuracy ($\beta = 0.020$, $p = 0.077$, generalized linear-mixed effects model). These results suggest that stronger SN/VTA engagement during cue evaluation may predict better reward-related performance. No effect of cue size was found, likely due to the delayed-target

presentation (see Figure 1D), which may have reduced the immediate behavioral impact of physical salience.

To further probe whether attention mediates the interaction between physical salience and stimulus evaluation, we analyzed alpha suppression—an established EEG marker of attentional engagement.[39–41] Alpha power (8–12 Hz) was extracted from electrodes linked to the late evaluative EEG component (Figure 1E). This allowed us to test whether attentional engagement, modulated by physical salience, enhanced subsequent stimulus evaluation.

We found stronger alpha suppression for large reward-predictive cues compared with large no-reward cues in the 725–900 ms post-cue window ($p < 0.05$, cluster-based permutation test corrected; Figure 5B). This effect was not present for small cues, suggesting that stimulus evaluation was mostly enhanced when physical salience and reward expectancy were aligned—likely through increased attention. Supporting this, alpha suppression slopes were steeper for large reward-predictive cues than for large no-reward cues ($t(23) = -2.6$, $p = 0.026$, paired t test on estimated individual slopes), but did not differ between small-reward and small no-reward cues ($t(23) = -0.45$, $p = 0.66$, paired t test on estimated individual slopes). These findings suggest more rapid and sustained attentional engagement when physical salience and reward were aligned. Additionally, greater alpha suppression at cue onset predicted faster response times across trials ($\beta = 0.0028$, $p = 0.010$), reinforcing its role as a marker of attentional readiness in reward processing.

Together, our findings support a pathway in which early physical salience boosts attentional engagement, which in turn facilitates later stimulus evaluation and may ultimately improve reward-guided behavior.

DISCUSSION

In this study, we used simultaneous EEG and 7T fMRI to temporally and spatially decouple physical salience and evaluation-related signals in the human midbrain during reward anticipation. Our data are highly consistent with the two-component dopaminergic reward response[1] and further extend it by suggesting that these signals are also spatially distinct within the midbrain.

The major advances of this work are 2-fold—theoretical and methodological. Theoretically, we show that reward responses evolve rapidly and sequentially in distinct midbrain locations, starting with unselective physical salience detection and quickly progressing to the more task-specific stage of stimulus evaluation. This sequence may reflect an adaptive mechanism in which physically salient stimuli are prioritized for further processing, possibly via attentional reorientation. More broadly, these findings substantiate previous proposals that dopamine midbrain signals incorporate information that goes beyond value.[42,43] Methodologically, combining EEG with 7T fMRI opens avenues for high spatiotemporal resolution imaging of small subcortical structures, offering new insights into the neural basis of human reward-guided behavior.

We observed an early physical salience signal, followed by a temporally lagged signal associated with stimulus evaluation. Crucially, these signals were not only temporally distinct but also spatially separated in the midbrain: early salience-related activity was localized to posterior-lateral SN, whereas later evaluation-related activity emerged more anteriorly in SN and VTA. We also observed a spatial gradient in the right SN/VTA, transitioning from physical salience to stimulus evaluation along a posterior-lateral to anterior-medial axis, which further supports a possible functional organization. Together, these findings suggest a functional topography in the human midbrain in which physical salience and stimulus evaluation are not only temporally but also spatially segregated. Importantly, this provides a critical empirical extension to the two-component dopaminergic reward framework, which has so far made only temporal predictions.[1] Here, we show that this framework can be expanded to include spatial segregation of early and late reward signals in the human midbrain.

Although our approach cannot isolate the impact of physical salience and stimulus evaluation on individual dopamine neurons, it suggests a spatial organization in the midbrain where predominantly salience-sensitive and valuation-sensitive neurons are likely segregated. Such spatial differentiation could reflect differences in the relative coding strength of the early and late components across dopamine neuron subpopulations[44] and may shape downstream effects in striatal targets based on their topographically organized midbrain inputs.[6,27]

Our findings help reconcile divergent perspectives from the non-human literature. For example, the multiphasic temporal dynamics described by Fiorillo et al.[2,4] suggest a time-based progression from physical salience to value, while Matsumoto and Hikosaka propose a spatial dissociation between motivational salience and value signals.[5] Our study brings these views together: we show that both temporal and spatial segregation may coexist in the human SN/VTA during reward anticipation, offering a more integrated model of midbrain functioning.

It is important to note that our design did not orthogonally manipulate value and motivational salience, as reward-predictive cues likely elicit both when compared with no-reward predictive cues. We therefore interpret the late signal as reflecting stimulus evaluation more broadly—a process that may include both value and motivational salience. Still, the spatial localization of this late signal to anterior-medial SN and VTA is more consistent with prior findings on value coding,[5,6,16] though we cannot entirely rule out additional contributions from motivational salience. Supporting this, we ran an independent EEG study showing that reward- and punishment-predictive cues—matched for motivational salience—could be discriminated based on late EEG signals, suggesting some value encoding in the late evaluative response.

Ultimately, future EEG-fMRI work using both reward and punishment outcomes will be necessary to fully dissociate these dimensions within the SN/VTA. Similarly, our observation that physical salience maps to posterior-lateral SN—overlapping with previously reported regions for motivational salience[5]—raises the possibility that both evaluation-agnostic and evaluation-based salience signals may converge on shared midbrain structures. This remains an open question and highlights the need for future studies to dissociate different forms of salience in the human midbrain.

In examining physical salience, we varied the size of reward-predictive cues and observed an early, unselective midbrain response, consistent with prior work showing that diverse forms

of physical salience (e.g., sounds, shocks, air puffs, and light flashes) elicit a rapid dopaminergic burst.[2,37,45–47] We also found that larger, more physically salient stimuli evoked faster immediate behavioral responses, suggesting that this early signal may help reorient attention toward relevant cues and facilitate subsequent stimulus evaluation. Indeed, we observed a positive coupling between early salience-related activity and later evaluative responses in the VTA, supporting the idea that salience signals may prime evaluative processing. Thus, while the two responses are temporally and spatially distinct, they are functionally interconnected within the midbrain, likely via attentional mechanisms.

Our findings support a role for dopaminergic SN signals in human attentional control. Alpha suppression—an established EEG marker of attentional engagement[39–41]—was stronger for physically salient reward-predictive cues, suggesting that salience-related SN activity helps prioritize relevant reward stimuli by capturing attention. This attentional function is likely shaped by inputs from other brainstem regions, such as the superior colliculus and locus coeruleus, which are sensitive to salient visual events and project directly to the SN.[36,48,49] Such inputs could boost SN activity for physically salient stimuli, thereby facilitating their subsequent evaluation in the VTA. It is also possible that attentional and reward-related signals are integrated within the midbrain before being broadcast to cortical areas as a unified prioritization signal, enhancing the processing of reward-predictive stimuli and improving behavioral accuracy.[50–52] Importantly, such a mechanism could optimize the balance between speed and accuracy,[1] linking attentional engagement to more efficient reward learning and action selection.

The sequential and rapid progression from physical salience to stimulus evaluation may also extend to other forms of human reinforcement and explain why aversive stimuli, such as shocks or monetary losses, sometimes activate dopamine-rich brain areas[53–57] and other times suppress it.[58–60] Activations could reflect the early, unselective salience signal, which responds to attention-capturing or physically salient stimulus (aversive or rewarding), while suppressions might represent the late evaluative response, which reflects negative value.[1,2] While our paradigm offers evidence for a two-component midbrain reward response, it would be interesting to further extend it to the punishment domain to further clarify these seemingly conflicting findings in human studies.

In many human fMRI studies, fast-changing physical salience and stimulus evaluation are likely conflated into an aggregate reward response due to the sluggish nature of the BOLD signal, leading to potentially inaccurate interpretations of brain processes. Here, by decoupling these distinct signals, we highlight the importance of combining temporally and spatially sensitive neuroimaging approaches in parsing midbrain activity. This fine-grained separation not only helps us better understand subcortical neurotransmitter pathways involved in reward processing but also provides insights into the specific disruptions underlying these pathways in mental health. Such insights can, in turn, help inform targeted interventions by pinpointing specific disruptions in physical salience processing and/or subsequent stimulus evaluation in mental health disorders.[61–63]

RESOURCE AVAILABILITY

Lead contact

Requests for further information and resources should be directed to and will be fulfilled by the lead contact, Joana Carvalheiro (joana.carvalheiro@glasgow.ac.uk).

Materials availability

This study did not generate new, unique reagents.

Data and code availability

- All data reported in this paper will be shared by the lead contact upon request.
- Original code for the linear discriminant analysis has been deposited at Zenodo and is publicly available as of the date of publication. DOI is listed in the key resources table.
- Any additional information required to reanalyze the data reported in this paper is available from the lead contact upon request.

ACKNOWLEDGMENTS

We thank Wolfram Schultz for insightful discussions on the study's conceptualization, interpretation, and the manuscript. We thank Frances Crabbe for supporting us with sequence optimization and data collection and Angus Paton for discussions on registration pipelines. This work was supported by the European Research Council (ERC, DyNeRfusion, 865003; M.G.P.) and partially supported by the John Robertson Bequest Fund, University of Glasgow (J.C.).

AUTHOR CONTRIBUTIONS

Conceptualization: J.C. and M.G.P.; methodology: J.C., P.M., S.A.-S., G.P., S.G., and M.G.P.; investigation: J.C.; formal analysis: J.C. and M.G.P.; visualization: J.C.; software: J.C. and M.G.P.; funding acquisition: J.C. and M.G.P.; project administration: M.G.P.; writing – original draft: J.C. and M.G.P.; writing – review and editing: J.C., P.M., S.A.-S., S.G., G.P., and M.G.P.

DECLARATION OF INTERESTS

In addition to his role at the University of Glasgow, S.G. is the founder and a shareholder of MR CoilTech Limited.

STAR★METHODS

Detailed methods are provided in the online version of this paper and include the following:

- KEY RESOURCES TABLE
- EXPERIMENTAL MODEL AND STUDY PARTICIPANT DETAILS
  - Participants
- METHOD DETAILS
  - Reward-anticipation EEG-fMRI task
  - Cue-size behavioural task
  - EEG-only control task
  - EEG data acquisition during concurrent fMRI
  - MRI data acquisition
- QUANTIFICATION AND STATISTICAL ANALYSIS
  - Behavioural analysis
  - EEG data preprocessing
  - Single-trial EEG analysis
  - fMRI preprocessing
  - Standard fMRI analysis
  - EEG-informed fMRI analysis
  - Regions of interest and corrections for multiple comparisons
  - Spatial SN/VTA gradient
  - Psychophysiological interaction analysis
  - Associations between stimulus evaluation and behavioural performance
  - Alpha power analysis

SUPPLEMENTAL INFORMATION

Supplemental information can be found online at https://doi.org/10.1016/j.cub.2025.09.013.

Received: June 2, 2025
Revised: August 11, 2025
Accepted: September 3, 2025
Published: September 30, 2025

REFERENCES

1. Schultz, W. (2016). Dopamine reward prediction-error signalling: a two-component response. Nat. Rev. Neurosci. *17*, 183–195. https://doi.org/10.1038/nrn.2015.26.
2. Fiorillo, C.D., Song, M.R., and Yun, S.R. (2013). Multiphasic temporal dynamics in responses of midbrain dopamine neurons to appetitive and aversive stimuli. J. Neurosci. *33*, 4710–4725. https://doi.org/10.1523/JNEUROSCI.3883-12.2013.
3. Eshel, N., Tian, J., Bukwich, M., and Uchida, N. (2016). Dopamine neurons share common response function for reward prediction error. Nat. Neurosci. *19*, 479–486. https://doi.org/10.1038/nn.4239.
4. Fiorillo, C.D., Yun, S.R., and Song, M.R. (2013). Diversity and homogeneity in responses of midbrain dopamine neurons. J. Neurosci. *33*, 4693–4709. https://doi.org/10.1523/JNEUROSCI.3886-12.2013.
5. Matsumoto, M., and Hikosaka, O. (2009). Two types of dopamine neuron distinctly convey positive and negative motivational signals. Nature *459*, 837–841. https://doi.org/10.1038/nature08028.
6. Cox, J., and Witten, I.B. (2019). Striatal circuits for reward learning and decision-making. Nat. Rev. Neurosci. *20*, 482–494. https://doi.org/10.1038/s41583-019-0189-2.
7. Murray, S.O., Boyaci, H., and Kersten, D. (2006). The representation of perceived angular size in human primary visual cortex. Nat. Neurosci. *9*, 429–434. https://doi.org/10.1038/nn1641.
8. Johannes, S., Münte, T.F., Heinze, H.J., and Mangun, G.R. (1995). Luminance and spatial attention effects on early visual processing. Brain Res. Cogn. Brain Res. *2*, 189–205. https://doi.org/10.1016/0926-6410(95)90008-X.
9. Carvalheiro, J., and Philiastides, M.G. (2023). Distinct spatiotemporal brainstem pathways of outcome valence during reward- and punishment-based learning. Cell Rep. *42*, 113589. https://doi.org/10.1016/j.celrep.2023.113589.
10. Lou, B., Hsu, W.-Y., and Sajda, P. (2015). Perceptual salience and reward both influence feedback-related neural activity arising from choice. J. Neurosci. *35*, 13064–13075. https://doi.org/10.1523/JNEUROSCI.1601-15.2015.
11. Zheng, Y., and Mei, S. (2023). Neural dissociation between reward and salience prediction errors through the lens of optimistic bias. Hum. Brain Mapp. *44*, 4545–4560. https://doi.org/10.1002/hbm.26398.
12. Hird, E.J., El-Deredy, W., Jones, A., and Talmi, D. (2018). Temporal dissociation of salience and prediction error responses to appetitive and aversive taste. Psychophysiology *55*, e12976. https://doi.org/10.1111/psyp.12976.
13. Stewardson, H.J., and Sambrook, T.D. (2021). Reward, salience, and agency in event-related potentials for appetitive and aversive contexts. Cereb. Cortex *31*, 5006–5014. https://doi.org/10.1093/cercor/bhab137.
14. Jensen, J., Smith, A.J., Willeit, M., Crawley, A.P., Mikulis, D.J., Vitcu, I., and Kapur, S. (2007). Separate brain regions code for salience vs. valence during reward prediction in humans. Hum. Brain Mapp. *28*, 294–302. https://doi.org/10.1002/hbm.20274.
15. Limbrick-Oldfield, E.H., Leech, R., Wise, R.J.S., and Ungless, M.A. (2019). Financial gain- and loss-related BOLD signals in the human ventral tegmental area and substantia nigra pars compacta. Eur. J. Neurosci. *49*, 1196–1209. https://doi.org/10.1111/ejn.14288.
16. Zhang, Y., Larcher, K.M.-H., Misic, B., and Dagher, A. (2017). Anatomical and functional organization of the human substantia nigra and its connections. eLife *6*, e26653. https://doi.org/10.7554/eLife.26653.
17. Richter, A., Reinhard, F., Kraemer, B., and Gruber, O. (2020). A high-resolution fMRI approach to characterize functionally distinct neural pathways within dopaminergic midbrain and nucleus accumbens during reward and salience processing. Eur. Neuropsychopharmacol. *36*, 137–150. https://doi.org/10.1016/j.euroneuro.2020.05.005.
18. Cooper, J.C., and Knutson, B. (2008). Valence and salience contribute to nucleus accumbens activation. NeuroImage *39*, 538–547. https://doi.org/10.1016/j.neuroimage.2007.08.009.
19. Hall, J.M., Shahnazian, D., and Krebs, R.M. (2024). Exploring distinct and joint contributions of the locus coeruleus and the substantia nigra/ventral tegmental area complex to reward and valence processing using high-resolution fMRI. Imaging Neurosci. (Camb) *2*, imag-2-00336. https://doi.org/10.1162/imag_a_00336.
20. Kahnt, T., and Tobler, P.N. (2013). Salience signals in the right temporoparietal junction facilitate value-based decisions. J. Neurosci. *33*, 863–869. https://doi.org/10.1523/JNEUROSCI.3531-12.2013.
21. Mcelhinney, P., Allwood-Spiers, S., Paterson, G., Philiastides, M., and Gunamony, S. (2021). Numerical modelling of a close-fitting 8-channel transceiver head coil and EEG electrodes for safety validation at 7T. ISMRM 2021 Annual Meeting. https://eprints.gla.ac.uk/236132/.
22. Parra, L.C., Spence, C.D., Gerson, A.D., and Sajda, P. (2005). Recipes for the linear analysis of EEG. Neuroimage *28*, 326–341. https://doi.org/10.1016/j.neuroimage.2005.05.032.
23. Sajda, P., Philiastides, M.G., and Parra, L.C. (2009). Single-trial analysis of neuroimaging data: inferring neural networks underlying perceptual decision-making in the human brain. IEEE Rev. Biomed. Eng. *2*, 97–109. https://doi.org/10.1109/RBME.2009.2034535.
24. Fouragnan, E., Retzler, C., Mullinger, K., and Philiastides, M.G. (2015). Two spatiotemporally distinct value systems shape reward-based learning in the human brain. Nat. Commun. *6*, 8107. https://doi.org/10.1038/ncomms9107.
25. Gherman, S., and Philiastides, M.G. (2015). Neural representations of confidence emerge from the process of decision formation during perceptual choices. Neuroimage *106*, 134–143. https://doi.org/10.1016/j.neuroimage.2014.11.036.
26. Zubair, M., Murris, S.R., Isa, K., Onoe, H., Koshimizu, Y., Kobayashi, K., Vanduffel, W., and Isa, T. (2021). Divergent whole brain projections from the ventral midbrain in macaques. Cereb. Cortex *31*, 2913–2931. https://doi.org/10.1093/cercor/bhaa399.
27. Haber, S.N., and Knutson, B. (2010). The reward circuit: Linking primate anatomy and human imaging. Neuropsychopharmacology *35*, 4–26. https://doi.org/10.1038/npp.2009.129.
28. de Hollander, G., Keuken, M.C., van der Zwaag, W., Forstmann, B.U., and Trampel, R. (2017). Comparing functional MRI protocols for small, iron-rich basal ganglia nuclei such as the subthalamic nucleus at 7 T and 3 T. Hum. Brain Mapp. *38*, 3226–3248. https://doi.org/10.1002/hbm.23586.
29. Knutson, B., Westdorp, A., Kaiser, E., and Hommer, D. (2000). FMRI visualization of brain activity during a monetary incentive delay task. Neuroimage *12*, 20–27. https://doi.org/10.1006/nimg.2000.0593.
30. Schultz, W., Dayan, P., and Montague, P.R. (1997). A neural substrate of prediction and reward. Science *275*, 1593–1599. https://doi.org/10.1126/science.275.5306.1593.
31. Chelazzi, L., Perlato, A., Santandrea, E., and Della Libera, C. (2013). Rewards teach visual selective attention. Vision Res. *85*, 58–72. https://doi.org/10.1016/j.visres.2012.12.005.
32. Guitart-Masip, M., Chowdhury, R., Sharot, T., Dayan, P., Duzel, E., and Dolan, R.J. (2012). Action controls dopaminergic enhancement of reward representations. Proc. Natl. Acad. Sci. USA *109*, 7511–7516. https://doi.org/10.1073/pnas.1202229109.

33. Knutson, B., Bhanji, J.P., Cooney, R.E., Atlas, L.Y., and Gotlib, I.H. (2008). Neural responses to monetary incentives in major depression. Biol. Psychiatry *63*, 686–692. https://doi.org/10.1016/j.biopsych.2007.07.023.

34. Itti, L., and Koch, C. (2001). Computational modelling of visual attention. Nat. Rev. Neurosci. *2*, 194–203. https://doi.org/10.1038/35058500.

35. Chen, Y., Chaudhary, S., and Li, C.-S.R. (2022). Shared and distinct neural activity during anticipation and outcome of win and loss: A meta-analysis of the monetary incentive delay task. NeuroImage *264*, 119764. https://doi.org/10.1016/j.neuroimage.2022.119764.

36. Comoli, E., Coizet, V., Boyes, J., Bolam, J.P., Canteras, N.S., Quirk, R.H., Overton, P.G., and Redgrave, P. (2003). A direct projection from superior colliculus to substantia nigra for detecting salient visual events. Nat. Neurosci. *6*, 974–980. https://doi.org/10.1038/nn1113.

37. Dommett, E., Coizet, V., Blaha, C.D., Martindale, J., Lefebvre, V., Walton, N., Mayhew, J.E.W., Overton, P.G., and Redgrave, P. (2005). How visual stimuli activate dopaminergic neurons at short latency. Science *307*, 1476–1479. https://doi.org/10.1126/science.1107026.

38. Bromberg-Martin, E.S., Matsumoto, M., and Hikosaka, O. (2010). Dopamine in motivational control: rewarding, aversive, and alerting. Neuron *68*, 815–834. https://doi.org/10.1016/j.neuron.2010.11.022.

39. Vázquez Marrufo, M., Vaquero, E., Cardoso, M.J., and Gómez, C.M. (2001). Temporal evolution of alpha and beta bands during visual spatial attention. Brain Res. Cogn. Brain Res. *12*, 315–320. https://doi.org/10.1016/s0926-6410(01)00025-8.

40. Thut, G., Nietzel, A., Brandt, S.A., and Pascual-Leone, A. (2006). α-band electroencephalographic activity over occipital cortex indexes visuospatial attention bias and predicts visual target detection. J. Neurosci. *26*, 9494–9502. https://doi.org/10.1523/JNEUROSCI.0875-06.2006.

41. Woodman, G.F., Wang, S., Sutterer, D.W., Reinhart, R.M.G., and Fukuda, K. (2022). Alpha suppression indexes a spotlight of visual-spatial attention that can shine on both perceptual and memory representations. Psychon. Bull. Rev. *29*, 681–698. https://doi.org/10.3758/s13423-021-02034-4.

42. Kahnt, T., and Schoenbaum, G. (2025). The curious case of dopaminergic prediction errors and learning associative information beyond value. Nat. Rev. Neurosci. *26*, 169–178. https://doi.org/10.1038/s41583-024-00898-8.

43. Gershman, S.J., Assad, J.A., Datta, S.R., Linderman, S.W., Sabatini, B.L., Uchida, N., and Wilbrecht, L. (2024). Explaining dopamine through prediction errors and beyond. Nat. Neurosci. *27*, 1645–1655. https://doi.org/10.1038/s41593-024-01705-4.

44. Dabney, W., Kurth-Nelson, Z., Uchida, N., Starkweather, C.K., Hassabis, D., Munos, R., and Botvinick, M. (2020). A distributional code for value in dopamine-based reinforcement learning. Nature *577*, 671–675. https://doi.org/10.1038/s41586-019-1924-6.

45. Horvitz, J.C. (2000). Mesolimbocortical and nigrostriatal dopamine responses to salient non-reward events. Neuroscience *96*, 651–656. https://doi.org/10.1016/S0306-4522(00)00019-1.

46. Horvitz, J.C., Stewart, T., and Jacobs, B.L. (1997). Burst activity of ventral tegmental dopamine neurons is elicited by sensory stimuli in the awake cat. Brain Res. *759*, 251–258. https://doi.org/10.1016/s0006-8993(97)00265-5.

47. Ljungberg, T., Apicella, P., and Schultz, W. (1992). Responses of monkey dopamine neurons during learning of behavioral reactions. J. Neurophysiol. *67*, 145–163. https://doi.org/10.1152/jn.1992.67.1.145.

48. Collingridge, G.L., James, T.A., and MacLeod, N.K. (1979). Neurochemical and electrophysiological evidence for a projection from the locus coeruleus to the substantia nigra [proceedings]. J. Physiol. *290*, 44P.

49. Sara, S.J. (2009). The locus coeruleus and noradrenergic modulation of cognition. Nat. Rev. Neurosci. *10*, 211–223. https://doi.org/10.1038/nrn2573.

50. Bushnell, M.C., Goldberg, M.E., and Robinson, D.L. (1981). Behavioral enhancement of visual responses in monkey cerebral cortex. I. Modulation in posterior parietal cortex related to selective visual attention. J. Neurophysiol. *46*, 755–772. https://doi.org/10.1152/jn.1981.46.4.755.

51. Treue, S., and Maunsell, J.H. (1996). Attentional modulation of visual motion processing in cortical areas MT and MST. Nature *382*, 539–541. https://doi.org/10.1038/382539a0.

52. Nardo, D., Santangelo, V., and Macaluso, E. (2011). Stimulus-driven orienting of visuo-spatial attention in complex dynamic environments. Neuron *69*, 1015–1028. https://doi.org/10.1016/j.neuron.2011.02.020.

53. Hennigan, K., D'Ardenne, K., and McClure, S.M. (2015). Distinct midbrain and habenula pathways are involved in processing aversive events in humans. J. Neurosci. *35*, 198–208. https://doi.org/10.1523/JNEUROSCI.0927-14.2015.

54. Seymour, B., O'Doherty, J.P., Koltzenburg, M., Wiech, K., Frackowiak, R., Friston, K., and Dolan, R. (2005). Opponent appetitive-aversive neural processes underlie predictive learning of pain relief. Nat. Neurosci. *8*, 1234–1240. https://doi.org/10.1038/nn1527.

55. Seymour, B., Daw, N., Dayan, P., Singer, T., and Dolan, R. (2007). Differential encoding of losses and gains in the human striatum. J. Neurosci. *27*, 4826–4831. https://doi.org/10.1523/JNEUROSCI.0400-07.2007.

56. Becerra, L., Breiter, H.C., Wise, R., Gonzalez, R.G., and Borsook, D. (2001). Reward circuitry activation by noxious thermal stimuli. Neuron *32*, 927–946. https://doi.org/10.1016/s0896-6273(01)00533-5.

57. Jensen, J., McIntosh, A.R., Crawley, A.P., Mikulis, D.J., Remington, G., and Kapur, S. (2003). Direct activation of the ventral striatum in anticipation of aversive stimuli. Neuron *40*, 1251–1257. https://doi.org/10.1016/s0896-6273(03)00724-4.

58. Tom, S.M., Fox, C.R., Trepel, C., and Poldrack, R.A. (2007). The neural basis of loss aversion in decision-making under risk. Science *315*, 515–518. https://doi.org/10.1126/science.1134239.

59. Seymour, B., Maruyama, M., and De Martino, B. (2015). When is a loss a loss? Excitatory and inhibitory processes in loss-related decision-making. Curr. Opin. Behav. Sci. *5*, 122–127. https://doi.org/10.1016/j.cobeha.2015.09.003.

60. Delgado, M.R., Li, J., Schiller, D., and Phelps, E.A. (2008). The role of the striatum in aversive learning and aversive prediction errors. Philos. Trans. R. Soc. Lond. B Biol. Sci. *363*, 3787–3800. https://doi.org/10.1098/rstb.2008.0161.

61. Heinz, A., and Schlagenhauf, F. (2010). Dopaminergic dysfunction in schizophrenia: salience attribution revisited. Schizophr. Bull. *36*, 472–485. https://doi.org/10.1093/schbul/sbq031.

62. Kesby, J.P., Murray, G.K., and Knolle, F. (2023). Neural circuitry of salience and reward processing in psychosis. Biol. Psychiatry Glob. Open Sci. *3*, 33–46. https://doi.org/10.1016/j.bpsgos.2021.12.003.

63. Robinson, T.E., and Berridge, K.C. (1993). The neural basis of drug craving: an incentive-sensitization theory of addiction. Brain Res. Brain Res. Rev. *18*, 247–291. https://doi.org/10.1016/0165-0173(93)90013-p.

64. Woolrich, M.W., Ripley, B.D., Brady, M., and Smith, S.M. (2001). Temporal autocorrelation in univariate linear modeling of FMRI data. Neuroimage *14*, 1370–1386. https://doi.org/10.1006/nimg.2001.0931.

65. Jenkinson, M., Bannister, P., Brady, M., and Smith, S. (2002). Improved optimization for the robust and accurate linear registration and motion correction of brain images. NeuroImage *17*, 825–841. https://doi.org/10.1016/s1053-8119(02)91132-8.

66. Andersson, J.L.R., Jenkinson, M., and Smith, S. (2007). Non-linear registration aka Spatial normalisation. https://www.fmrib.ox.ac.uk/datasets/techrep/tr07ja2/tr07ja2.pdf.

67. Friston, K.J., Ashburner, J., Kiebel, S., Nichols, T., and Penny, W. (2007). Statistical Parametric Mapping: the Analysis of Functional Brain Images, First Edition (Elsevier/Academic Press).

68. Cox, R.W., Chen, G., Glen, D.R., Reynolds, R.C., and Taylor, P.A. (2017). fMRI clustering and false-positive rates. Proc. Natl. Acad. Sci. USA *114*, E3370–E3371. https://doi.org/10.1073/pnas.1614961114.

69. Oostenveld, R., Fries, P., Maris, E., and Schoffelen, J.-M. (2011). FieldTrip: Open source software for advanced analysis of MEG, EEG, and invasive electrophysiological data. Comput. Intell. Neurosci. *2011*, 156869. https://doi.org/10.1155/2011/156869.

70. Peirce, J.W. (2009). Generating stimuli for neuroscience using PsychoPy. Front. Neuroinform. *2*, 10. https://doi.org/10.3389/neuro.11.010.2008.

71. Brain Products GmbH (2021). BrainVision Recorder. Version 1.20 (Brain Products).

72. The MathWorks, Inc. (2021). MATLAB. Version R2021a (MathWorks).

73. Duda, R.O., Hart, P.E., and Stork, D.G. (2000). Pattern Classification, Second Edition (John Wiley & Sons).

74. Bianciardi, M., Strong, C., Toschi, N., Edlow, B.L., Fischl, B., Brown, E.N., Rosen, B.R., and Wald, L.L. (2018). A probabilistic template of human mesopontine tegmental nuclei from *in vivo* 7T MRI. NeuroImage *170*, 222–230. https://doi.org/10.1016/j.neuroimage.2017.04.070.

75. Mitra, P.P., and Pesaran, B. (1999). Analysis of dynamic brain imaging data. Biophys. J. *76*, 691–708. https://doi.org/10.1016/S0006-3495(99)77236-X.

CellPress
OPEN ACCESS

STAR★METHODS

KEY RESOURCES TABLE

REAGENT or RESOURCE	SOURCE	IDENTIFIER
Software and algorithms		
Custom computer code for linear discriminant analysis	Zenodo	https://doi.org/10.5281/zenodo.14006241
FSL	University of Oxford[64–66]	https://fsl.fmrib.ox.ac.uk/fsl/fslwiki
SPM12	Wellcome Trust Centre for Neuroimaging, UCL[67]	https://www.fil.ion.ucl.ac.uk/spm/software/spm12/
AFNI 3dClustSim	National Institutes of Health[68]	https://afni.nimh.nih.gov/pub/dist/doc/program_help/3dClustSim.html
MRIcroGL	Chris Rorden	https://www.nitrc.org/projects/mricrogl
EEGLAB v14.1.2.	Delorme and Makeig	https://sccn.ucsd.edu/eeglab/index.php
FieldTrip	Donders Institute for Brain, Cognition and Behaviour[69]	https://www.fieldtriptoolbox.org/
Psychopy2	Pierce[70]	https://www.psychopy.org/
Brain Vision Recorder	Brain Products[71]	https://brainvision.com/products/recorder/
MATLAB R2021a	MathWorks[72]	https://www.mathworks.com/products/matlab.html
Other		
MR-compatible EEG amplifier system	BrainAmps MR-Plus, Brain Products	N/A
MR-compatible EEG customized cap	64Ch BrainCap-MR with Multitrodes, Brain Products	N/A
Siemens 7-Tesla Terra MRI scanner	Siemens	N/A
Custom-built MRI head coil 8-channel transceiver array	Mcelhinney et al.[21]	N/A

EXPERIMENTAL MODEL AND STUDY PARTICIPANT DETAILS

Participants

Twenty-four participants (20 females and 4 males) aged 19 to 36 years (mean age = 24 years, standard deviation = ± 4.6) took part in the simultaneous 7T fMRI-EEG experiment reported here. These participants were selected from a pool of thirty-seven participants who were tested for a separate stand-alone EEG study (using the same task as in this study), designed to explore the relationship between EEG and the cardiac cycle. The subset selected for this study was based solely on head size from 54 to 56 cm, in order to fit in our custom-built 7TfMRI-EEG head coil.

Our target sample size was a minimum of 22 participants. This number is consistent with previous 7T MRI studies focusing on subcortical and midbrain regions, where sample sizes typically range from 20 to 25 participants due to the higher signal-to-noise ratio and the technical and logistical constraints of ultra-high field imaging.[28] Moreover, a physical salience signal was observed in 86% of participants in the stand-alone EEG study, indicating a robust and reliable neural response, likely reflecting a large effect size and supports the adequacy of our sample size for detecting relevant midbrain salience-related activity.

For the secondary cue-size behavioural task, 26 participants were initially recruited. Two were excluded due to poor performance (accuracy below 10% in at least one condition), resulting in a final sample of 24 participants. This sample size was determined a priori based on a G*Power analysis for a paired-sample t-test designed to detect an interaction effect — specifically, the difference in reaction times between large and small stimuli in the cue (immediate) task versus the delayed target task — assuming a moderate effect size (d = 0.6) and 80% power. This also allowed us to match the sample size of our main EEG-fMRI cohort for consistency across tasks.

For the EEG-only control task, 24 participants (19 females and 5 males, mean age = 24 years, standard deviation = ± 4.8) were recruited to parallel the EEG-fMRI sample size, as the analysis targeted similar signals.

All participants were right handed, had normal or corrected-to-normal vision with contact lenses and reported no history of psychiatric, neurological or major medical problems, and were free of psychoactive medications at the time of the study. This study used a mixed sample of male and female participants as we had no a priori reason to predict differences between sexes. The study was approved by the College of Medical, Veterinary & Life Sciences at the University of Glasgow (200220183) and informed consent was obtained from all participants.

METHOD DETAILS

Reward-anticipation EEG-fMRI task

The experiment was a modified version of the monetary incentive delay task,[29] consisting of 4 blocks of 36 trials each (144 total), with breaks between blocks. In half of the trials, participants observed a coloured circle (blue or yellow) predicting either a reward (£10) or no-reward (£0). Within each condition (reward or no-reward), circles independently varied in size (small: ~1 cm, large: ~3 cm in diameter, based on initial design specifications created for visual composition on a 27-inch monitor, 2560 × 1440 resolution; ~43 pixels/cm), yielding 72 pseudorandomised trials per condition. This design ensured an orthogonal manipulation of size (physical salience) and reward expectancy (stimulus evaluation). Circle colours were equiluminant and respective outcomes were counterbalanced across participants.

Each trial began with a fixation cross (1 - 4 seconds; mean = 2.5 seconds), followed by a coloured circle for 1 second. After a 1-3 seconds delay (mean = 2 seconds), participants pressed a key as quickly as possible to hit a target (white square), which appeared briefly (0.1-0.5 seconds, adjusted by a 2-down 1-up staircase procedure). Participants hit the target on 67% (± 4%) of trials on average. Following each trial, the outcome was displayed for 0.75 s. Hitting the target after a reward-predictive cue yielded a £10 outcome, while a miss resulted in £0. For the no-reward predictive cue, the outcome was always £0, but participants were instructed to still respond as quickly as possible. The task was presented using Psychopy2.[70]

Participants completed a practice block in the MRI (no functional data collected) to consolidate the deterministic cue-outcome associations, with reaction times in the last practice trials used as reference for the first task trials. They were informed they would receive a base payment (£15) and could win up to an additional £20 based on the selection of a random subset of trials; all participants received £30.

Cue-size behavioural task

This secondary behavioural experiment was designed to validate whether our physical salience manipulation effectively captured greater attention and modulated reaction times. The experiment included two conditions, presented in a counterbalanced and alternating order across four blocks (72 trials per block). Stimuli consisted of blue and yellow circles, presented in a pseudorandomised order. On half of the trials, circles were large, and on the other half, small—ensuring that size was orthogonal to colour, as in the main task. Participants were instructed to respond only to circles of a specific colour (either blue or yellow), with the assigned colour counterbalanced across participants.

In the immediate-cue response condition, participants pressed a key as quickly as possible when a circle of the specific colour appeared, regardless of its size. Each circle was shown for 1 second and followed by a fixation cross lasting 1–3 seconds, replicating the timing of the main EEG-fMRI task. In the delayed-target response condition, participants did not respond to the circle directly. Instead, a staircase-calibrated target (white square), presented for 0.1–0.5 seconds, appeared 1–3 seconds after each circle, and participants responded to this subsequent target. This condition matched the delayed-response design of the EEG-fMRI task. To isolate the effects of physical salience, correct responses were neither rewarded nor followed by any feedback.

EEG-only control task

To assess whether our late EEG evaluative component reflected stimulus value, motivational salience, or both, we conducted a standalone EEG experiment in an independent sample. To keep this control task feasible and not overly long, all cues were physically matched in size (equivalent to the 'large' cues in the main EEG-fMRI task). Importantly, in addition to reward- and neutral-predictive cues, this version included punishment-predictive cues allowing us to isolate effects of value (reward versus punishment) and motivational salience (reward+punishment versus neutral). Each cue type (reward-, neutral- or punishment-predictive) was distinguished by different colour (equiluminent and counterbalanced across participants) and presented for 1 second, as in the main task.

Participants could win one point for hitting the target after a reward-predictive cue (or receive nothing if they missed), lose one point for missing after a punishment-predictive cue (or avoid losing by hitting), or receive no outcome after a neutral-predictive cue. They were instructed to respond as quickly as possible to not miss the delayed target on all trials. Feedback was displayed for 0.75 seconds, consistent with the EEG-fMRI task. Each participant completed 72 trials per cue type (216 trials total), divided across six blocks.

EEG was recorded with a 64-channel Ag/AgCl cap (Brain Products), using the international 10–20 system, identical to the EEG-fMRI setup (see below). Data were analysed using the same multivariate discriminant pipeline as in the main experiment (see Figure S2).

EEG data acquisition during concurrent fMRI

EEG was recorded simultaneously with the fMRI data using an MR-compatible EEG amplifier system (BrainAmps MR-Plus, Brain Products) and recorded using Brain Vision Recorder (Brain Products)[71] with a 5-kHz sampling rate. Data were filtered online with a hardware band-pass filter of 0.016–250 Hz. The EEG cap (Brain Products) was customised for 7T MRI and included 64 Ag/AgCl scalp electrodes which were localised according to the international 10–20 system. All electrodes had in-line 5 kΩ surface-mount resistors to ensure participant safety, which was further guaranteed by bundling and twisting all leads for their entire length. We designed the EEG caps to have a pigtail length of 20 cm to ensure the shortest possible direct path to the EEG amplifiers in order to minimise inductive pick-up and MR-related EEG artifacts. We lowered the input impedance for each electrode to <50 kΩ.

EEG and MRI data acquisition were synchronised with a Syncbox (Brain Products), and scanner triggers were separately recorded for later gradient artifact removal. An in-house pulse stretcher extended scanner pulses to 50 ms. Experimental event codes and participant responses were recorded in sync with EEG data in Brain Vision Recorder. The MRI helium pumps were turned off during acquisition to reduce EEG artifacts.

MRI data acquisition

Simultaneous EEG-fMRI data were acquired using a Siemens 7-Tesla Magnetom Terra scanner at the Imaging Centre of Excellence, University of Glasgow with an in-house 8-channel transceiver array head coil[21] (Figure 2A) driven in circularly polarised mode using a 1×8 power splitter.

To target the midbrain, T2*-weighted echo planar images (EPIs) were acquired, covering the midbrain, upper pons, and parts of the striatum (see Figure S3A). The EPI sequences were modified from de Hollander et al.[28] to ensure safe EEG-fMRI acquisition. We set Specific Absorption Rate (SAR) limits based on the EEG amplifier manufacturer's (Brain Products) recommendations regarding sequence parameters. For the 8-channel head coil, this resulted in a SAR limit of 34% of normal mode, 3.4 W/kg local SAR (compared to a normal mode limit of 10 W/kg for local SAR). Each T2*-weighted EPI volume consisted of 32 slices in an interleaved-ascending order, with a 1.5 mm isotropic resolution. Imaging parameters included: TR = 2000 ms, TE = 14 ms, flip angle = 70° (adjusted to 65° in 8/24 participants, when SAR levels exceeded safety limits), field of view = 192 × 192 mm, matrix = 128 × 128, GRAPPA factor = 3, and bandwidth = 1446 Hz/Px. A T1-weighted MP2RAGE anatomical scan (1 mm isotropic resolution) was acquired using a 32-channel coil (Nova Medical Inc.) prior to EEG-fMRI to facilitate EPI co-registration to MNI space.

QUANTIFICATION AND STATISTICAL ANALYSIS

Behavioural analysis

For the main EEG-fMRI task, reaction times were compared following rewarded versus non-rewarded cues (collapsed across large and small cues). Mean reaction times were calculated for each participant and analysed using paired t-tests. A similar analysis compared reaction times following large versus small cues (collapsed across reward and no-reward predictive cues).

For the secondary behavioural cue-size task, reaction times were analysed by comparing responses to large versus small cues, for the immediate-cue and delayed-target response tasks. Only trials in which participants correctly responded to the assigned colour were included in the analysis (immediate cue task: 1721/1728 trials, delayed target task: 1173/1728 trials). Mean reaction times were calculated for each participant and submitted to a repeated-measures ANOVA with factors of cue size (large, small) and response condition (immediate, delayed), followed by paired t-tests to probe significant effects.

Effect sizes are reported as Cohen's d for paired t-tests and partial η^2 for the ANOVA interaction.

EEG data preprocessing

EEG data was preprocessed offline using MATLAB (Mathworks).[72] EEG signals recorded inside an MR scanner are contaminated with gradient and ballistocardiogram (BCG) artifacts due to magnetic induction on the EEG leads. To address these artifacts, we applied several preprocessing steps.

Gradient artifacts were removed by constructing templates from sets of 80 consecutive functional volumes centred on each volume of interest and subtracting these from the EEG signal, repeated for each volume in the dataset. Residual spikes were removed with a 10-ms median filter, and signals were band-pass filtered (0.5 - 40 Hz Butterworth filters) to eliminate slow direct current drifts and high-frequency noise. Data were then downsampled to 1000 Hz.

To remove eye blinks, participants completed an eye-blinking calibration task in the scanner. Blink events were recorded and identified in the EEG using principal component analysis (PCA), and blink-related components were removed from task data.

For BCG artifact correction, a conservative PCA approach was applied to remove between 1 and 4 BCG components per participant, to minimise the possibility of removing physiologically relevant signals.[24] We relied on our multivariate discriminant analysis (see below), which was designed to tolerate small residual artifacts that are not systematically aligned to experimental events of interest.[9] BCG principal components were extracted after the data were low-pass filtered at 4 Hz to extract the signal within the frequency range where most of the BCG power residues. Next, subject-specific principal components were determined based on the number of components that achieved the best accuracy on a single-trial classifier for the physical salience and stimulus evaluation components, within the interval 100–600 ms post-cue onset (average number of components was 3 for salience and stimulus evaluation). These components were projected onto the original broadband data and subtracted out. Data quality, validated by comparing the accuracy of the decoder with a 3TfMRI-EEG dataset (where BCG artifacts are lower), was sufficient for subsequent analyses (see Figure S3D).

Single-trial EEG analysis

We applied a single-trial multivariate discriminant analysis with a sliding window approach[22,23] to discriminate between large versus small trials (physical salience component), and reward versus no-reward trials (stimulus evaluation component) in the EEG data locked to the time of the cue. For each participant, we concatenated data across the four blocks. This method calculates an optimal linear combination of EEG sensor weights (spatial filter) within predefined time windows, generating a one-dimensional discriminant

component $y\,(t)$ from the multichannel EEG data $x\,(t)$. This component enables discrimination between large and small cues (collapsed across reward and no-reward) or between reward and no-reward cues (collapsed across large and small size),

$$y\,(t) = w^T x\,(t) = \sum_{s=1}^{D} w_s x_s\,(t), \qquad \text{(Equation 1)}$$

where D represents the number of channels (here 64), indexed by s, and T denotes the transpose of the matrix. We estimated spatial weights w using a sliding window approach, with short (60 ms) overlapping time windows, centered at 10 ms increments from −100 and 1000 ms relative to cue onset. Trials when participants pressed prematurely for the cue, were excluded (45 out 3456 trials). This analysis was conducted independently for each participant, time window, and component (salience or evaluation). Applying w to an individual trial yielded discriminant component amplitudes $y\,(t)$, with spatial filters designed to assign positive values to large and reward cue trials and negative values to small and no-reward cue trials; note, however, that this mapping is arbitrary.

To estimate the optimal discriminating spatial weighting vector w we used a regularised Fisher discriminant analysis as follows: $w = S_c(m_2 - m_1)$, where $m_i$is the estimated mean of condition i and $S_c = 1/2(S_1 + S_2)$ (is the estimated common covariance matrix (i.e., the average of the condition-wise empirical covariance matrices, $S_i = 1/(n-1)\sum_{j=1}^{n}(x_j - m_i)(x_j - m_i)^T$, with n = number of trials). We replaced the condition-wise covariance matrices with regularised versions of these matrices to counteract potential estimation errors: $\tilde{S}_i = (1-\lambda)S_i + \lambda\nu I$, with $\lambda \in [0, 1]$ being the regularisation term and ν the average eigenvalue of the original S_i [i.e., *trace* (S_i/D), with D corresponding to the dimensionality of the EEG space]. Note that $\lambda = 0$yields unregularised estimation and $\lambda = 1$ assumes spherical covariance matrices. We optimised λ using leave-one-trial-out cross validation in two steps. First, $\lambda$was tested from 0 to 0.4 in 0.05 increments. Next, the optimisation range was refined using increments of 0.001, within ± 0.05 of the λ value that maximised discrimination in a generously defined cue-locked window of interest (between 100 and 600 ms post cue, where we expected the discriminator to peak) for each component in the initial step. We applied the optimal λ from this final step in the linear discriminant analysis (mean λ ± s.d.: 0.15 ± 0.19).

To quantify the performance of the discriminator for each time window, we computed the area under a receiver operating characteristic (ROC) curve (i.e., the A_z value), using a leave-one-out-trial cross-validation procedure.[73] Specifically, for every iteration, we used N-1 trials to estimate a spatial filter w, which was then applied to the remaining trial to obtain out-of-sample discriminant component amplitudes, y (separately for physical salience and stimulus evaluation; see Figure S1) and compute the A_z. We used this approach to identify discrimination performance during different time windows, and used the resultant single-trial component amplitudes, $y\,(t)$, to build parametrically modulated BOLD predictors for our fMRI analysis.

The linearity of our model also allows computing scalp projections of the relevant discriminating components resulting from Equation 1 by estimating a forward model for each component:

$$a = \frac{Xy}{y^T y} \qquad \text{(Equation 2)}$$

where the EEG data X and discriminating components y are now in a matrix and vector notation, respectively (i.e., both X and y now contain a time dimension). Equation 2 describes the electrical coupling of the discriminating component y that explains most of the activity in X. Strong coupling indicates low attenuation of the component y and can be visualised as the intensity of vector a. The resulting scalp topographies were used to visualise distinct spatial profiles for each component, which is typically indicative of distinct neural generators.

To identify time points where decoding accuracy exceeded chance ($A_z > 0.5$), we used FieldTrip's[69] ft_timelockstatistics function to perform a cluster-based permutation test. A one-sample right-tailed t-test was conducted against chance level ($A_z = 0.5$) for each component's A_z time course (−100 to 1000 ms, in 10 ms steps). Temporally adjacent samples with $P < 0.05$ were grouped into clusters (cluster-forming threshold $\alpha = 0.05$), and cluster-level significance was determined by comparing the observed cluster statistics to a null distribution generated from 1,000 permutations. Clusters were deemed significant if their test statistic exceeded the 99th percentile of the null distribution (one-tailed cluster-level $\alpha = 0.01$), thereby correcting for multiple comparisons across time.

fMRI preprocessing

MRI data preprocessing was conducted for each block (158 volumes) using the FEAT tool from the FSL software (FMRIB Software Library).[64] This process included slice-timing correction, high-pass filtering (>100 s), and spatial smoothing with a 3 mm Gaussian kernel. Brain extraction from EPIs was performed using the Brain Extraction Tool (BET), while structural images (inverted T1-weighted images) were segmented using SPM (version 12).[67]

Each exemplar EPI from each block was linearly registered to the exemplar EPI from the first block, and these transformations were applied to all EPIs to align them in the same individual space. We co-registered the EPIs to the anatomical space using SPM. The resulting transformations from SPM were input into the linear registration in FSL to enhance the alignment of EPIs to the T1-weighted space (FLIRT command in FSL).[65] T1-weighted images were transformed into MNI (Montreal Neurological Institute) space using the Non-linear Image Registration Tool (FNIRT command in FSL)[66] with a 10 mm warp resolution. This transform was combined with the EPIs to T1-weighted space transformation and applied to all EPIs. Registration quality was visually inspected, and manual adjustments were made to transformation matrices in three participants to improve SN/VTA alignment.

To address the challenges of registering small field-of-views at 7T, we implemented quality checks. First, the SN was manually delineated in the individual transforms from EPI to MNI space generated at the second level (after averaging across all blocks for

each participant). We performed this manual delineation on two separate occasions, and only overlapping voxels were retained for the final individual masks, which were then binarised and summed across participants to create a probability mask. Second, we quantified the percentage of overlapping voxels between the individual manually delineated SN masks and the SN mask derived from the Brainstem Navigator Atlas.[74] On average, manually delineated individual registrations of the SN showed a 77% overlap with the SN mask in the standard space, with 23 out of 24 participants overlapping at the peak (Figure 2B). Finally, all individual transforms from EPI to MNI space were summed for visual inspection, indicating good alignment (Figure 2C).

Standard fMRI analysis

We first performed a conventional (non EEG-informed) fMRI analysis to identify differences in midbrain responses to physical salience and stimulus evaluation. A separate General Linear Model (GLM) was set up for each block, locking the regressors of interest at cue onset. Each GLM included two boxcar regressors of interest, both with a duration of 1000 ms to match the cue duration: (1) a categorical regressor for physical salience, where large cues were coded as 1 and small cues as -1, (2) a categorical regressor for stimulus evaluation-related signals, where reward cues were coded as 1 and no-reward cues as -1. Additionally, we included several regressors of no interest: a boxcar regressor for target modelled with reaction times (or target duration for missed target responses), a regressor for the outcome, a regressor for premature responses at cue onset, and six nuisance regressors corresponding to head motion parameters (three rotations and three translations). Contrasts were performed at the first level for each of the two categorical regressors (physical salience and stimulus evaluation), followed by combination across the four blocks at the second level, and finally aggregation at the group level using a mixed-model (FLAME 1).

EEG-informed fMRI analysis

In our main EEG-fMRI analysis, we exploited the EEG single-trial-variability in the physical salience and stimulus evaluation components to build EEG-informed fMRI regressors. Specifically, we used the trial-by-trial amplitude estimates of $y\ (t)$ (Equation 1) for each component, averaged in 60 ms windows from 100–600 ms to capture the period of peak EEG-relevant activity and minimise noise from early and late non-specific activations.

We replaced the two categorical regressors for large > small (physical salience) and reward > no-reward (stimulus evaluation) in the standard GLM with corresponding parametric EEG-informed regressors. This yielded sixteen regressors of interest in total: eight time windows for physical salience and eight for stimulus evaluation. All parametric EEG-informed regressors were time-locked to cue onset, irrespective of the time window from which the EEG amplitudes were extracted. We also added an unmodulated regressor of no interest at cue onset to account for activations unrelated to the parametric EEG-informed regressors. The rest of the design was identical to the standard GLM described above.

We performed first-level contrasts for physical salience and stimulus evaluation within each time window, which were entered into second-level analyses to combine all blocks, and finally combined across all subjects at group-level.

As an additional control, we confirmed that retaining the categorical regressors for physical salience and stimulus evaluation in the EEG-fMRI analysis did not alter the interpretation of our main clusters at 160–220 ms and 400–460 ms, respectively.

Regions of interest and corrections for multiple comparisons

Our analyses focused on the SN/VTA, midbrain subregions implicated in reward anticipation in electrophysiological studies with non-human subjects.[5,6,30] The SN/VTA mask was built from adding probabilistic bilateral masks for SN and VTA from the Brainstem Navigator Atlas[74] (total voxels: 664, 2 mm isotropic). We did not apply a threshold on top of the original atlas masks, to accommodate potential deviations in the registration of the EPIs to MNI space. However, we confirmed that applying a threshold of 35% to the SN/VTA mask did not alter the interpretation of our main EEG-fMRI clusters.

To balance sensitivity and specificity in these very small, low–signal-to-noise nuclei at 7T, we adopted a voxel-wise cluster-defining threshold of $P < 0.01$ ($Z > 2.3$) combined with cluster-level family-wise error correction ($P < 0.05$) within the anatomically defined SN/VTA mask. We then used AFNI's 3dClustSim[68] to perform 10,000 Monte Carlo simulations—accounting for our SN/VTA search volume and smoothing kernel—to determine the minimum cluster extent at our chosen voxel-wise threshold. Across simulations, a cluster size of 7 voxels was required to achieve $P < 0.05$ FWE within the SN/VTA mask.

As a robustness check, we used to same approach to confirm that all reported SN/VTA clusters survived a more conservative threshold of $P < 0.005$ ($Z > 2.58$).

Spatial SN/VTA gradient

We calculated the voxel-wise difference between group-level Z-scored fMRI maps for physical salience (160–220 ms) and stimulus evaluation (400–460 ms), based on time windows identified in the EEG-fMRI analysis. These Z-score differences were extracted for all voxels within the anatomical SN/VTA mask, separately for left and right hemispheres. To assess the spatial profile along the posterior-anterior axis, Z-scores were binned along the Y-axis (MNI space) into 6 equally spaced intervals, and the mean Z-score difference was computed within each bin, producing a smoothed posterior-anterior activation gradient. To quantify the gradient, we performed separate linear regression analysis on the spatial profile for left and right SN/VTA. To test whether the spatial profiles differed significantly between hemispheres, we fit a linear model with an interaction term between hemisphere and Z-score difference. We then tested the lateral-to-medial gradient by repeating these analyses along the X-axis (MNI space).

Psychophysiological interaction analysis

We extracted BOLD time-series data from each individual's early physical salience clusters found in the EEG-fMRI analysis (those covarying with EEG activity at 160-220 ms post-cue), and used these clusters as seed regions (i.e., physiological regressor) in a psychophysiological interaction analysis (PPI). To extract the time-series data from subject-specific clusters, we back-projected the identified clusters at the group level in standard MNI space into each individual's EPI space by applying the inverse transformations estimated during registration (see STAR Methods, section "fMRI preprocessing"). For the psychological regressor, we used the EEG endogenous variability, $y(t)$ estimated for the later evaluation component between 400-460ms post-cue. This regressor allowed us to model the strength of association between BOLD activity in the early physical salience clusters and late SN/VTA clusters when amplitudes for stimulus evaluation in the EEG signal were stronger.

The PPI analyses included the following regressors: (1) the physiological regressor (BOLD time-series in the EEG-fMRI derived clusters that covaried with the EEG physical salience component at 160-220 ms post-cue), (2) the psychological regressor (EEG amplitudes corresponding to the late evaluation-related component, averaged between 400-460 ms post-cue) and (3) the interaction regressor (physiological $\times$ psychological). The rest of the design was otherwise identical to the EEG-informed GLM outlined previously. The interaction regressor was entered at the second level to combine all blocks.

We then extracted individual estimates from this interaction regressor within each of the three sub-clusters identified in our main EEG-fMRI analysis for the late stimulus evaluation component (those covarying with EEG activity at 400-460 ms post-cue), followed by one-sample t-tests against zero and paired t tests between the different sub-clusters, to assess the significance of these estimates.

Associations between stimulus evaluation and behavioural performance

To assess the behavioural relevance of midbrain activity during stimulus evaluation, we extracted trial-wise BOLD signals from the SN/VTA cluster that, in our EEG-informed fMRI analysis, covaried with the late evaluation-related EEG component (400–460 ms post-cue). The cluster was defined from group-level results and back-projected to the individual EPI space. For each participant and trial, we extracted the mean BOLD signal from this region for 14 seconds post-cue onset (TR = 2 s), baseline-corrected relative to a pre-cue window (2 TRs), and normalised to each voxel's mean signal. This analysis was restricted to trials involving reward-predictive cues, where accuracy was higher. Each trial was labelled as correct if the participant responded to the target within the allotted time, or as missed if they failed to do so. We averaged BOLD time courses over the 0–14 seconds post-cue window and compared them between correct and missed trials using a Wilcoxon signed-rank test (which is more robust to individual deviations in the BOLD signal) across participants. To assess whether BOLD activity predicted performance at the trial level, we fitted a generalised linear mixed-effects model using the mean post-cue signal (0–14 seconds) as a predictor of binary accuracy (correct or missed), with random intercepts per subject.

Alpha power analysis

We examined alpha-band (8–12 Hz) suppression to assess attentional engagement across conditions. Time-frequency decomposition of EEG data was performed at the single-trial level using the multitaper method[75] implemented in the FieldTrip toolbox,[69] applied to cue-locked EEG data from -500 to 1200 ms. A fixed sliding time window of 400 ms and frequency smoothing of ±4 Hz were used with orthogonal Slepian tapers. This approach provides robust spectral estimates for signals with low signal-to-noise ratio, such as those in the alpha range.[75]

Analysis focused on three centroparietal electrodes (CP2, CP4, C2), selected based on maximal discrimination weights in the EEG topography of the late stimulus evaluation component (Figure 1E). Alpha power values were baseline-corrected by computing the percentage change from a 400 ms pre-cue window, yielding relative rather than absolute power estimates.Trials were then split into four conditions based on cue size and reward expectancy (large reward, large no-reward, small reward, small no-reward).

To assess condition differences in alpha suppression over time, we used FieldTrip's[69] ft_timelockstatistics function to perform a cluster-based permutation test on the alpha power time course. At each time point, two-tailed paired-samples t-tests compared alpha power for large-reward versus small-reward cues. Temporally adjacent samples with $p < 0.05$ were grouped into clusters (cluster-forming threshold $\alpha = 0.05$). Cluster-level significance was evaluated against a null distribution generated from 1,000 permutations. Clusters were deemed significant if their test statistic exceeded the 97.5th percentile (positive or negative tail) of the null distribution (cluster-level $\alpha = 0.05$, two-tailed), thereby correcting for multiple comparisons across time.

To assess the temporal dynamics of alpha suppression, we computed subject-specific linear slopes of alpha power from 100 to 900 ms post-cue for each cue type, and compared them across subjects using paired t-tests.

Aditionally, to validate alpha suppression as a marker of attentional readiness, we tested whether trial-wise alpha power predicted response times to the delayed target following reward-predictive cues, using a generalised linear mixed-effects model with subject-level random intercepts.